Spectral–Spatial Classification With Naive Bayes and Adaptive FFT for Improved Classification Accuracy of Hyperspectral Images

Arvind Kumar Singh, Renuvenkataswamy Sunkara, *Graduate Student Member, IEEE*, Govind R. Kadambi, and Vasile Palade, *Senior Member, IEEE*

***Abstract*—This article presents a postprocessing-based spectral–spatial classification (SSC) approach for hyperspectral (HS) images. The approach effectively overcomes the limitations of traditional pixel-based classifiers by integrating spectral and spatial information to achieve improved classification results. Specifically, the proposed method uses principal component analysis to transform the HS images and the Naive Bayes (NB) classifier to quickly derive spectral-posterior probabilities. Spatial-posterior probabilities are then computed using an adaptive fast Fourier transform (AFFT) and a probabilistic closeness function. These probabilities are then combined to generate a precise SSC map. The proposed approach is available in two distinct styles: the conventional NB–AFFT–SSC method and the proposed iterationwise variable sequencing based NB–AFFT–SSC (IVS–NB–AFFT–SSC) method, which classifies one designated class in each iteration. In addition, two wrapper-based feature selection methods are proposed to obtain a set of principal components (PCs) for each class of the HS image, significantly improving classification accuracy. The approach's efficacy is demonstrated through extensive experimentation on three real HS datasets, including Washington DC Mall, Salinas-A, and Botswana. The generality of the approach has been proven through the use of other well-known machine-learning algorithms, such as support vector machine and K-nearest neighbor, as wrappers in the approach. The results confirm that the proposed approach is highly effective, with the IVS approach helping users concentrate on a particular set of PCs for the class of interest.**

***Index Terms*—Adaptive fast Fourier transform (AFFT), hyperspectral (HS) image, spectral–spatial classification (SSC), iterationwise variable sequencing (IVS), Naive Bayes (NB).**

I. Introduction

HYPERSPECTRAL (HS) images are rich in information and are essential in land cover, land use, climate, and environmental applications. Classification is one of the significant tasks in HS image processing. The methods that utilize the spectral signature to determine class belongingness are called pixel-based classifiers, for example, Bayesian estimation methods [1], K-nearest neighbor (KNN) classifiers [2], kernel-based techniques [3], neural networks [4], and decision trees [5]. The performance of pixel-based classifiers is limited due to high heterogeneity within the same class and relatively more homogeneity between pixels of different classes of the HS image, which arise due to high spatial resolution [6], natural spectrum variations, unwanted shade and shadow, atmospheric effects, incident illumination, and instrument noises [7] during the image acquisition. Therefore, the classification maps produced by the pixel-based classifiers exhibit salt and pepper noise. Moreover, the classification performance of pixel-based classifiers has a strong relationship with the quality of training pixels [8]. As pixel-based classifiers do not consider spatial information, they cannot alone constitute good classifiers. Therefore, the need for spectral–spatial classification (SSC) arises. In the literature, based on the fusion stage, three categories of SSC were proposed for HS images, such as preprocessing techniques as in [9] and [10], where the spatial information is pre-extracted before being fed to the classifier, integrated techniques [11], [12], where spatial information and spectral information are simultaneously used without explicit separation, and postprocessing techniques [13], [14], [15], [16], [17], where spectral information via a classifier and spatial information mostly using Markov random fields are extracted, which lead to computational overhead and over smoothening.

Recently, the focus of SSC of HS images has been shifted to deep learning (DL)-based methods and has become the mainstream [18], [19]. The advantage of DL methods is that they do not require dimensionality reduction, feature selection (FS), or a combination of spatial–spectral information exclusively for the SSC of HS images. Due to this advantage, a series of DL methods have emerged for HS image classification [20]. For example, the two-dimensional convolutional neural network (2-DCNN) method is used for SSC of HS images, which suffers from significant performance degradation as the training data drop from 20% to 3%, as shown in [21]. Another DL method that is widely used and considered a state-of-the-art (SOTA) is the 3-DCNN, which extracts both spectral and spatial information, and it offers better execution speed and performance

Manuscript received 24 May 2023; revised 1 September 2023; accepted 8 October 2023. Date of publication 25 October 2023; date of current version 8 December 2023. *(Corresponding author: Renuvenkataswamy Sunkara.)*

Arvind Kumar Singh is with the CATVAC Department, U R Rao Satellite Centre, Bengaluru 560017, India (e-mail: arksingh@hotmail.com).

Renuvenkataswamy Sunkara is with the CATVAC Department, U R Rao Satellite Centre, Bengaluru 560017, India (e-mail: renu.electronics@gmail.com).

Govind R. Kadambi is with the Department of Research, MS Ramaiah University of Applied Sciences, Bangalore 560054, India (e-mail: pvc2@msruas.ac.in).

Vasile Palade is with the Research Center for Computational Science and Mathematical Modeling, Coventry University, CV1 5FB Coventry, U.K. (e-mail: ab5839@coventry.ac.uk).

Digital Object Identifier 10.1109/JSTARS.2023.3327346

than 2-DCNN [21], [22], [23]. In addition, various CNN-based methods with the combination of 2-DCNN and 3-DCNN are being explored for better classification accuracy of HS images. A common need for all these methods is the requirement of a higher percentage of training data for a reasonably good classification performance.

Unlike conventional image processing applications, it is well known that in HS image processing, there is a scarcity of availability of sufficient training data or one cannot have the luxury or leverage of using a higher percentage of available data for training purposes alone [24]. The labeling of pixels in HS images is particularly time-consuming and expensive. The task requires experts to obtain ground-truth data by field sampling. Therefore, exploring an HS image classification methodology for good performance with few labeled samples becomes particularly significant [25]. Further in DL methods, generative adversarial networks (GANs) that combine the benefits of CNNs and the generative models are used to improve classification performance with few labeled samples [26]. However, the GANs suffer from the class imbalance problem due to the uncontrolled generation of synthetic training samples. In the context of the limited availability of training samples and the high dimensional nature of HS image data, DL methods perform quite ineffective in generalizing the distribution of HS image data. In addition, DL methods require excessive adjustment at the training stage, while the performance on the test data is generally poor with a low percentage of training data [20]. Moreover, the block box nature of the training of DL models makes the interpretation of internal dynamics quite hard. Further, the stacking of layers in DL methods does not guarantee desirable improvement in classification accuracy. This forces the users to carefully select the DL methods that best suit the HS image data. This involves a proper selection of the DL architecture, learning strategy, and improvement strategies that best fit the HS image data, which makes them dataset-specific, handcrafted, and complex. In addition, a high computational burden due to a large number of parameters that need to be maintained in a DL architecture demands computationally expensive and memory-intensive methods [27]. Hence, the exploration of the SSC approach devoid of DL models that work with a low percentage of training data for improved classification accuracy of HS images is the main focus of the article. It may be noted that the HS image and HS dataset are interchangeably used in the article.

The proposed SSC approach adopts the postprocessing-based approach, which is widely used among the three categories for the classification of HS images mainly due to higher classification accuracy and also attempts to address the computational overhead issue. Initially, the given HS image is transformed into a lower dimension using principal component analysis (PCA), as this is a widely used dimensionality reduction technique for HS images [17]. The rationale for the choice of PCA is that the usage of Naive Bayes (NB) insists on conditional independence of features to be fed as an input. In the proposed SSC approach, the spectral information in terms of posterior probabilities is obtained by the NB classifier, which is selected due to its inherent advantages, such as implementation ease, execution speed, and less complexity [28], [29], whereas the spatial information in terms of posterior probabilities is obtained through the application of an adaptive fast Fourier transform (AFFT) on a defined spatial window. The window-based method is an effective and widely used method to describe spatial information [30], [31]. In the proposed method, spectral posterior probabilities and spatial posterior probabilities are combined to obtain spectral–spatial posterior probabilities to construct the SSC map.

The proposed SSC approach has been implemented in two ways: 1) the conventional approach of classification, where the classification of all classes of the HS image is carried out at one shot and the method is named NB–AFFT–SSC; and 2) the proposed iterationwise variable sequencing (IVS) approach, where only one designated class of the HS image is classified in each iteration and the method is named as IVS–NB–AFFT–SSC. The proposed IVS approach is iterative and each iteration is designated with a class index as per the predefined class selection sequence. In addition, each iteration is wrapped with a predetermined classifier (NB classifier), which produces a classification map. The pixels from the classification map that match with the iteration class index are extracted and the remaining pixels are then fed to the next iteration, and this process continues until all classes in the given HS image are classified. The proposed novel IVS approach serves the dual purpose of FS and classification of HS images. The proposed IVS approach obtains a set of principal components (PCs) for each class of the HS image when used for FS, and performs the classification using these PCs to improve the classification accuracy. In addition, two FS methods, namely include discard based feature selection (IDFS) and IVS–FS are proposed. The IDFS method wraps a classifier (NB classifier) and employs the sequential forward selection (SFS) to obtain a set of PCs for all classes of the HS image based on a defined criterion.

In contrast, the IVS–FS method is iterative and it wraps the NB classifier in each iteration and employs the SFS search strategy to obtain a set of PCs for each class of the HS image. The IVS–FS method helps the user select a set of relevant PCs for a class of interest for further processing, such as classification. The PCs obtained by IDFS are used for the classification using the NB–AFFT–SSC method, whereas a set of PCs for each class is used for the classification using the IVS–NB–AFFT–SSC method. To the best of our knowledge, there is no attempt toward the SSC of HS images using "a set of PCs for each class" or "classwise PCs." Experiments conducted on three widely used real HS datasets, namely Washington DC Mall (WDC-M) [32], Salinas-A [33], and Botswana [34], substantiate the effectiveness of the proposed SSC method in terms of classification accuracy of the HS datasets.

The major contributions of the article are as follows.

1) The IDFS method with an improved objective criterion for the selection of PCs for all classes of HS image is illustrated.
2) A unique IVS–FS method for classwise PC selection of HS images is introduced.
3) A flexible postprocessing-based SSC approach both in the conventional classification approach and IVS approach,

with an explanation related to concepts behind the derivation of spectral information (using NB) and spatial information (by the proposed closeness function through AFFT), is presented.

4) The generality of the proposed SSC approach using other machine-learning (ML) algorithms, such as the widely used support vector machine (SVM) [35] and KNN [36], is demonstrated.
5) A comparison of the proposed SSC approach based methods along with other competitive SSC methods to substantiate the effectiveness of the proposed SSC approach is also presented.

The rest of this article is organized as follows. Section II introduces the details of the proposed FS algorithms for the proposed SSC approach with NB classifier as wrapper. Section III presents the conceptual basis and formulation of the proposed SSC approach with NB classifier as wrapper. Section IV describes the datasets used for all simulations including other well-known ML algorithms, such as SVM and KNN, to prove the generalization ability of the proposed approach. Section V presents the experimental results followed by a detailed discussion on the obtained results. Finally, Section VI concludes this article.

II. Implementation of Proposed Feature Selection Algorithms for the Proposed SSC Approach

In a traditional sense, the selection of PCs is based on the cumulative variance of PCs. In classification algorithms, the class discrimination aspect is neglected in the selection of the number of PCs, and this in turn leads to poor classification results. Hence, the class discrimination aspect cannot be neglected in the selection of the number of PCs. The imposition of the threshold for the initial dominant PCs is aimed as a pragmatic measure to overcome the absence of the class discrimination aspect. The proposed FS algorithms, such as IDFS and IVS–FS, address these problems by searching for PCs beyond the first few PCs, while maintaining classification accuracy. The proposed FS algorithms use SFS as a search strategy. In SFS-based FS, the objective function considers only the overall accuracy (OA) for FS leading to the issue of nonconsideration of class imbalance. However, in IDFS and IVS–FS, the objective function is derived based on the confusion matrix. This in turn overcomes the prevalent class imbalance in the FS algorithms. This section introduces the implementation details of the proposed FS algorithms with the NB classifier as a wrapper in IDFS and IVS–FS to obtain a set of PCs for all classes of the HS image and to obtain a set of PCs for each class of the HS image, respectively.

A. IDFS

This section presents the proposed IDFS method (wrapped with NB classifier), which uses the SFS strategy.

For the illustration of the algorithm, let the PCA-transformed HS image be given by

$$P = \{p_z\}_{z=1}^{\mathrm{Z}} \tag{1}$$

where p_z is the zth PC of the HS image, Z is the total number of PCs, and P is the set of PCs.

Algorithm 1: Pseudocode for IDFS Method.

Inputs:
Principal Components : $P = \{p_z\}_{z=1}^{\mathrm{Z}}$
Training data : *train*
Holdout test data : *htest*
Method:
Initialize feature set R to zero and a variable η to ∞
for ($z = 1$; $z \leq$ Z; z^{++})
Update feature set $R_z = \{R \cup p_z\}$;
Execute the **NB_classifier**(*train, htest,* R_z)
Compute ψ_{R_z} using (3)
if $z > 1$
if ($\psi_{R_z} < \eta$)
Update $R = \{R_z\}$;
Update $\eta = \psi_{R_z}$;
else
Update $R = \{R_z - p_z\}$;
end
else
Update $\eta = \psi_{R_z}$;
Update $R = \{R_z\}$;
End
end
Assign $\mathcal{R} = R$;
Output:
A set of PCs: $\mathcal{R}$

The IDFS decision metric to either add a PC or discard a PC requires the confusion matrix. The confusion matrix for the holdout test set using the NB classification map with the zth candidate PC set (R_z) is given by

$$\mathbf{W}_{R_z} = \begin{bmatrix} w_{11} & w_{12} & w_{13} & \dots & \dots & w_{1k} \\ w_{21} & w_{22} & w_{23} & \dots & \dots & w_{2k} \\ \vdots & \vdots & \vdots & \vdots & \ddots & \vdots \\ w_{k1} & w_{k2} & w_{k3} & \dots & \dots & w_{kk} \end{bmatrix} \tag{2}$$

where w_{11} is the first class pixels correctly classified as first class, w_{21} represents the second class pixels incorrectly classified as first class, and w_{kk} is the kth class pixels correctly classified as kth class.

The decision metric for the zth candidate PC set (R_z), denoted by ψ_{R_z}, using (2), can be given by

$$\psi_{R_z} = \frac{\sum_{k=1,\ k\neq j}^{\mathrm{K}} w_{kj}}{\sum_{k=1}^{\mathrm{K}} w_{kk}}. \tag{3}$$

The set of PCs that minimizes (3) will be given by

$$\mathcal{R} = \underset{R_z \subseteq P,\ z=\{1,2,3,\dots,\mathrm{Z}\}}{\operatorname{argmin}} \psi_{R_z} \tag{4}$$

where $\mathcal{R}$ will have a set of PCs for all classes of the HS image.

The pseudocode of the proposed IDFS method is shown in Algorithm 1 for a better understanding of the method.

B. IVS–FS

This section presents the details of the proposed IVS–FS method. The IVS–FS is an iterative approach that uses the NB classifier as a wrapper in each iteration, employs the SFS search strategy, and requires a sequence of classes to obtain classwise PCs for each defined class of the HS image. The input image to the method is the PCA-transformed HS image. The output is the classwise PCs for each defined class of the HS image.

For the kth class iteration, using the zth candidate PC set (R_z^k), a classification map is produced by the NB classifier. However, for the computation of the confusion matrix, only the pixels that match with the kth class index are considered, and the resultant confusion matrix is given by

$$\mathbf{W}_{R_z^k} = \begin{bmatrix} w_{00} & w_{01} \\ w_{10} & w_{11} \end{bmatrix} \tag{5}$$

where w_{00} is the 0th class pixels correctly classified as 0th class, w_{01} denotes the 0th class pixels incorrectly classified as first class, w_{10} represents the first class pixels incorrectly classified as 0th class, and w_{11} is the first class pixels correctly classified as first class.

The IVS–FS decision metric at the kth class iteration and for the zth candidate PC set (R_z^k) using (5) can be given by

$$\psi_{R_z^k} = \frac{\sum_{i=0,\, i\neq j}^{1} w_{ij}}{\sum_{i=0}^{1} w_{ii}}. \tag{6}$$

The set of PCs that minimizes (6) for the kth iteration class will be given by

$$\mathcal{R}^k = \underset{R_z^k \subseteq P,\ z=\{1,2,3,\ldots,\mathrm{Z}\},\ k=\{1,2,3,\ldots,\mathrm{K}\}}{\operatorname{argmin}} \psi_{R_z^k} \tag{7}$$

where $\mathcal{R}^k$ represents a set of PCs for the kth class (classwise PCs). The pseudocode of the method is shown in Algorithm 2. To the best of our knowledge, obtaining classwise PCs has not yet been explored. Hence, the proposed IVS–FS method adds a major contribution to the article.

Algorithm 2: Pseudocode for IVS-FS Method.

Inputs:
Principal Components : $P = \{p_z\}_{z=1}^{\mathrm{Z}}$
Class selection sequence index : k
Total number of classes : K
Training data with class labels : *train*
Hold out test data : *htest*
Method:
Initialize R to zero and a variable η to ∞
Loop1: for ($k = 1$; $k \leq$ K; k^{++})
Loop2: for ($z = 1$; $z \leq$ Z; z^{++})
Update $R_z^k = \{R \cup p_z\}$;
Execute **NB_classifier** (*train, htest,* R_z^k)
Compute $\psi_{R_z^k}$ using (6)
if $z > 1$
if ($\psi_{R_z^k} < \eta$)
Update $R = \{R_z^k\}$;
Update $\eta = \psi_{R_z^k}$;
else
Update $R = \{R_z^k - p_z\}$;
end
else
Update $\eta = \psi_{R_z^k}$;
Update $R = \{R_z^k\}$;
end
end: Loop2
Assign $\mathcal{R}^k = R$;
Update *train* to consist of only $(\mathrm{K} - k)$ classes
Update *htest* by removing classified pixels belonging to k^{th} class
Update R to zero
end: Loop1
Output:
Class-wise PCs for each class index k: $\mathcal{R}^k$

III. Proposed SSC Approach—Conceptual Basis and Formulation

The proposed SSC approach considers both the spatial and spectral information separately. It employs the NB classifier to produce a spectral classification map using the spectral information. For accounting the spatial information, an AFFT-based probabilistic closeness function is developed. The spectral posterior probabilities produced by the NB classifier and the spatial posterior probabilities obtained using the AFFT are used to generate spectral–spatial posterior probabilities, which are subsequently used for developing the final SSC map. The test pixel which has the highest posterior probability for a class will be assigned to the class. The proposed SSC approach is implemented in two classification approaches, namely the conventional approach (where the classification of all constituent classes is performed at a time) and the IVS approach (where the classification is carried out by a predefined class sequence). The proposed SSC approach implemented in the conventional approach is named as NB–AFFT–SSC and that in the IVS approach is designated as IVS–NB–AFFT–SSC.

A. NB–AFFT–SSC Method

This section presents the NB–AFFT–SSC method. In this method, the NB classifier is used to generate spectral posterior probabilities, and then the AFFT on a defined spatial window is used to compute spatial posterior probabilities. The NB–AFFT–SSC method is depicted in Fig. 1.

For the PCA transformed HS image with K number of classes, the spectral posterior probabilities using the NB classifier for the kth class, given a data vector $\mathbf{x}_q = \{x_z\}_{z=1}^{\mathrm{Z}}$, where z is the index to denote the zth PC and q is the pixel number, can be obtained by

$$p_{\mathrm{spec}}(k|\mathbf{x}_q) = \frac{[p(k) \times p(\mathbf{x}_q|k)]}{\sum_{k=1}^{\mathrm{K}} [p(k) \times p(\mathbf{x}_q|k)]} \tag{8}$$

where k is the index to denote kth class ($k = \{1, 2, \ldots, \mathrm{K}\}$), $p_{\mathrm{spec}}(k|\mathbf{x}_q)$ represents the posterior probability of the pixel vector $\mathbf{x}_q$ belonging to the kth class, and $p(k)$ is the priori probability

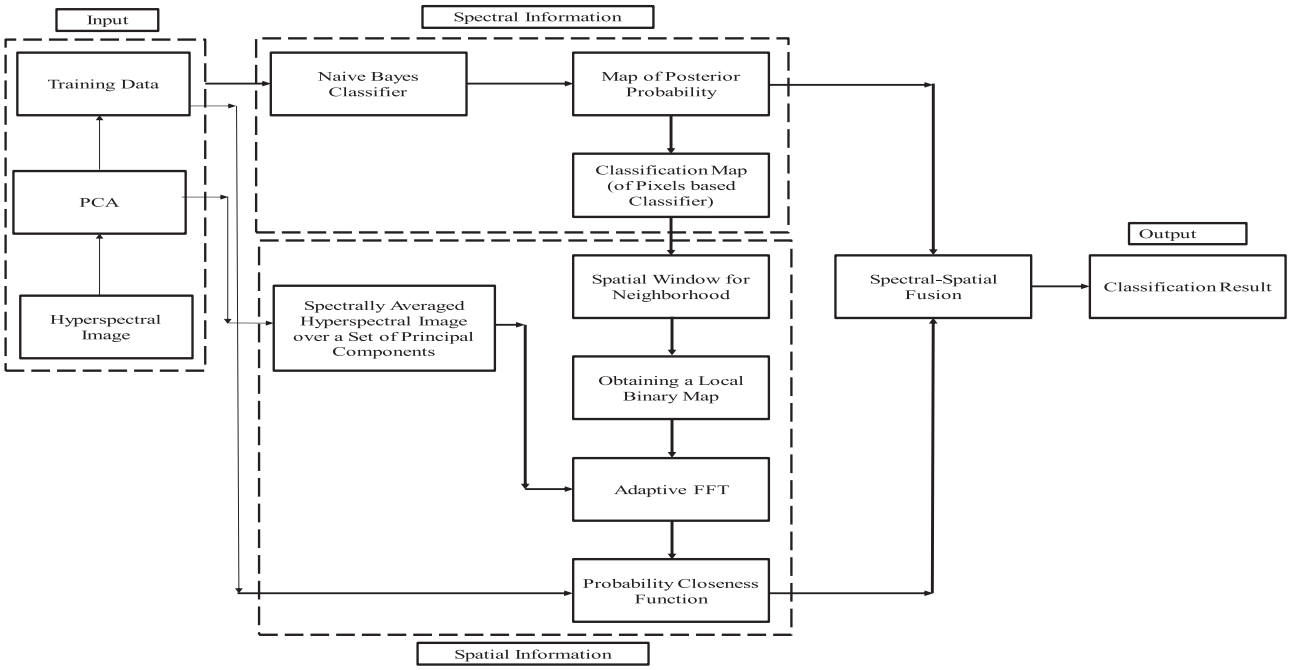

Fig. 1. Schematic of the proposed NB-AFFT-SSC method.

of the kth class. According to (9), each test pixel of the input HS dataset is assigned the class with which it has the highest posterior probability, and it can be given by

$$\mathbf{H}(\mathbf{x}_q) = \underset{k \in \{1\ to\ \mathrm{K}\}}{\arg\max}\ p_{\mathrm{spec}}\left(k|\mathbf{x}_q\right) \tag{9}$$

where $\mathbf{H}(\mathbf{x}_q)$ is the classification map of the class index for $\mathbf{x}_q$.

Using (9), a binary mask by comparing the center pixel $(\mathbf{x}_q)$ with the neighboring pixels of the defined spatial window is generated, which is multiplied element by element with the corresponding input PCA transformed HS image and then averaged over the selected PCs.

The FFT is applied adaptively on the averaged PCA transformed HS image of the size of spatial window, and the vector of test spectral magnitudes is denoted by $\mathbf{f}_{\mathrm{Test}}(\omega)$, where ω denotes the frequency component. A vector of FFT spectral magnitudes for training data, denoted by $\mathbf{f}_{\mathrm{Tr}}(\omega, k)$, is computed for each class k. The closeness function/metric for the kth class can then be calculated from [37]

$$\mathfrak{p}\left(k|\mathbf{x}_q\right) = \left| \frac{\mathbf{f}_{\mathrm{Tr}}\left(\omega, k\right)}{\mathbf{f}_{\mathrm{Test}}\left(\omega\right)} - \frac{\mathbf{f}_{\mathrm{Test}}\left(\omega\right)}{\mathbf{f}_{\mathrm{Tr}}\left(\omega, k\right)} \right|. \tag{10}$$

In (10), the value of ω is taken to be 1 (dc component) to reduce computational complexity. The ideal value for $\mathfrak{p}(k|\mathbf{x}_q)$ is zero. The value of $\mathfrak{p}(k|\mathbf{x}_q)$ can be any real value greater than zero (>0). Hence, it should be normalized as shown in (11), which is also called as probabilistic closeness function

$$\mathfrak{p}_{\mathrm{norm}}(k|\mathbf{x}_q) = \frac{\mathfrak{p}(k|\mathbf{x}_q)}{\sum_{k=1}^{\mathrm{K}} \mathfrak{p}(k|\mathbf{x}_q)} \tag{11}$$

where $k = 1$ to K such that $\sum_{k=1}^{\mathrm{K}} \mathfrak{p}_{\mathrm{norm}}(k|\mathbf{x}_q) = 1$.

The spatial posterior probabilities can be given by

$$p_{\mathrm{spat}}(k|\mathbf{x}_q) = \left(\frac{1 - \mathfrak{p}_{\mathrm{norm}}\left(k|\mathbf{x}_q\right)}{\sum_{k=1}^{\mathrm{K}} \left(1 - \mathfrak{p}_{\mathrm{norm}}\left(k|\mathbf{x}_q\right)\right)} \right). \tag{12}$$

Using (8) and (12), the spectral–spatial posterior probabilities can be computed using

$$\mathfrak{p}_{\mathrm{ss}}(k|\mathbf{x}_q) = p_{\mathrm{spec}}(k|\mathbf{x}_q) \times p_{\mathrm{spat}}(k|\mathbf{x}_q) \tag{13}$$

where $\mathfrak{p}_{\mathrm{ss}}(k|\mathbf{x}_q)$ represents the spectral–spatial posterior probabilities of the kth class given the pixel $\mathbf{x}_q$.

The SSC map can be obtained from

$$\boldsymbol{\mathcal{H}}(\mathbf{x}_q) = \underset{k \in \{1\ \mathrm{to}\ \mathrm{K}\}}{\arg\max}\ \mathfrak{p}_{\mathrm{ss}}\left(k|\mathbf{x}_q\right) \tag{14}$$

where $\boldsymbol{\mathcal{H}}(\mathbf{x}_q)$ is the SSC map of the predicted class index for $\mathbf{x}_q$.

B. IVS–NB–AFFT–SSC Method

This section presents the details of the IVS–NB–AFFT–SSC method, which uses the NB–AFFT–SSC method as a wrapper and uses classwise PCs obtained using the IVS–FS method. The schematic of the IVS–NB–AFFT–SSC method is shown in Fig. 2.

For example, if there are K number of classes, the integers in the class selection sequence will be $1 \leq i < \mathrm{K}$, implying that there are only $(\mathrm{K} - 1)$ steps of successive classification. The classification map at an iteration, for example, ith iteration, will be written as

$$\mathbf{C}_i^{\mathrm{K}-i+1} = \mathbf{CB}\left(train\left(\mathrm{K} - i + 1\right),\ test\left(\mathrm{K} - i + 1\right),\right.$$
$$\left.\mathcal{R}_i^*,\ \mathrm{NB} - \mathrm{AFFT} - \mathrm{SSC}\right). \tag{15}$$

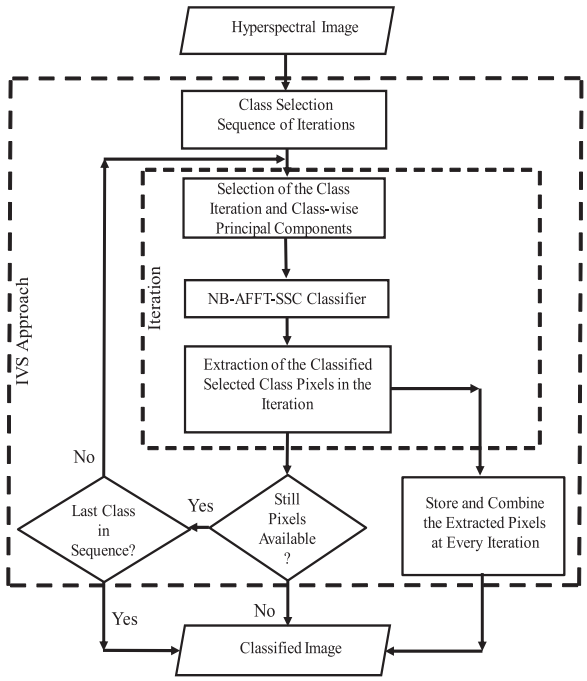

Fig. 2. Schematic of the proposed IVS–NB–AFFT–SSC method.

Let $p = \mathrm{K} - i + 1$ to simplify (15), which leads to

$$\mathbf{C}_i^p = \mathbf{CB}\left(train\left(p\right),\ test\left(p\right),\ \mathcal{R}_i^*,\ \mathrm{NB-AFFT-SSC}\right) \tag{16}$$

where p denotes the number of classes that are present, $train(p)$ represents the training data comprising p number of classes, $test(p)$ represents the test data comprising p number of classes, $\mathcal{R}_i^*$ represents a set of PCs at ith iteration, and the NB–AFFT–SSC method is a wrapper classifier. Now, the class index (i.e., k) corresponding to the ith iteration will have to be extracted from the classification map $\mathbf{C}_i^p$ in (16). The classification map of extracted kth class pixels is given by

$$\mathbf{H}^k = \begin{cases} \mathbf{C}_i^k \subset \mathbf{C}_i^p \mid k \in \mathbf{C}_i^p,\ 1 \leq k \leq \mathrm{K},\ \text{for } p > 2 \\ \mathbf{C}_i^k = \mathbf{C}_i^p,\ \text{otherwise} \end{cases} \tag{17}$$

where $\mathbf{H}^k$ is the classification map of kth class pixels. The classification map of the IVS–NB–AFFT–SSC method is given by

$$\mathbf{H}_{\mathrm{IVS-NB-AFFT-SSC}} = \sum_{k=1}^{\mathrm{K}} \mathbf{H}^k. \tag{18}$$

The iterative sequence of the classes can be either in ascending, descending, or predetermined order. The training data for both FS using the IVS–FS method and classification using the IVS–NB–AFFT–SSC method are the same.

IV. Datasets

The HS image datasets used for simulations are WDC-M [32], Salinas-A [33], and Botswana [34].

The actual size of WDC-M after the removal of water absorption bands is [1208 × 307 × 191]. The spatial resolution of the HS image is 2.5 m. We have considered a subscene of the WDC-M of size [99 × 306 × 191], which has seven classes, namely grass, water, street, roofs, trees, path, and shadow [32]. It is a challenging dataset due to the heterogeneity in the spectral signature of the roofs class and the low interclass spectral variability between the water–shadow, trees–grass, and roofs–street classes [38].

A subscene, named Salinas-A, of the Salinas scene captured by the AVIRIS sensor is another dataset used for simulations. The size of Salinas-A is [86 × 83 × 204]. The spatial resolution of Salinas-A is 3.7 m. There are six classes in Salinas-A HS image, which are named Brocoli_green_weeds_1, Corn_senesced_green_weeds, Lettuce_romaine_4wk, Lettuce_romaine_5wk, Lettuce_romaine_6wk, and Lettuce_romaine_7wk [33].

The third dataset used for simulations is the Botswana dataset from the NASA Earth Observing-1 satellite of the Okavango Delta, Botswana. After the noisy and water absorption band removal, the size of the image is [1476 × 256 × 145], which has 14 classes, namely, water, hippo grass, floodplain grasses1, floodplain grasses2, reeds1, riparian, firescar2, island interior, Acacia woodlands, Acacia shrublands, Acacia grasslands, short mopane, mixed mopane, and exposed soils [34].

V. Simulation Results and Discussion

This section presents the FS results of IDFS and IVS–FS methods, and the classification results of various representative algorithms along with SOTA and the proposed SSC methods for three real and widely used HS datasets, such as WDC-M, Salinas-A, and Botswana. A personal computer installed with MATLAB R2022a is used for all simulations on the datasets, with the following configuration: Processor: Intel(R) Core (TM) i3-4170 CPU @ 3.70 GHz, RAM: 4 GB, System type: 64-bit operating system with ×64 based processor. The selection of training pixels is random. However, one has the choice to decide the training data by selecting either uniformly or empirically for each class of the given HS dataset. The remaining pixels other than the training pixels of the HS image are used as testing pixels. The choice of the proportion of training data should be such that the classification method will be able to perform very well with the attribute of class discrimination feature in the dataset.

For simulations, a randomly selected training data of 2.5% for each HS dataset is used as shown in Table I for WDC-M, Salinas-A, and Botswana datasets. Five-fold cross-validation has been carried out for NB [29], SVM [35], and KNN [36]. The KNN with three nearest neighbors and the SVM with linear kernel are considered for simulations. For 3-DCNN [21], [22], [23], three 3-D convolutional layers are used. Each convolutional layer contains filter sizes 8, 16, and 32. The learning rate and epochs of 3-DCNN are set to 0.005 and 100, respectively.

A. Results of Proposed Feature Selection Algorithms

This section presents the details of the set of PCs obtained using both IDFS and IVS–FS methods with the NB classifier and also with other prominent ML algorithms, such as SVM and KNN alongside their execution times for the three HS

TABLE I
DATASETS USED FOR EXPERIMENTS

	WDC-M			Salinas-A			Botswana		
No.	Class	# of training pixels	# of test pixels	Class	# of training pixels	# of test pixels	Class	# of training pixels	# of test pixels
#1	Grass	143	5724	Brocoli_green_weeds_1	10	391	Water	7	270
#2	Water	121	4842	Corn_senesced_green_weeds	34	1343	Hippo grass	3	101
#3	Street	49	1973	Lettuce_romaine_4wk	15	616	Floodplain grasses1	6	251
#4	Roofs	4	158	Lettuce_romaine_5wk	38	1525	Floodplain grasses2	5	215
#5	Trees	41	1647	Lettuce_romaine_6wk	17	674	Reeds1	7	269
#6	Path	8	306	Lettuce_romaine_7wk	20	799	Riparian	7	269
#7	Shadow	3	99	–	–	–	Firescar2	7	259
#8	–	–	–	–	–	–	Island interior	5	203
#9	–	–	–	–	–	–	Acacia woodlands	8	314
#10	–	–	–	–	–	–	Acacia shrublands	6	248
#11	–	–	–	–	–	–	Acacia grasslands	8	305
#12	–	–	–	–	–	–	Short mopane	5	181
#13	–	–	–	–	–	–	Mixed mopane	7	268
#14	–	–	–	–	–	–	Exposed soils	2	95
# Total		369	14749	–	134	5348	–	83	3248

TABLE II
PCS OBTAINED BY PROPOSED FEATURE SELECTION ALGORITHMS WITH VARIOUS CLASSIFIERS FOR WDC-M HS DATASET

Method	Class	Selected PCs			Execution time (s)		
		SVM	NB	KNN	SVM	NB	KNN
IDFS	All classes	1:3,8,15,20,106,107,122	1:3,5,13,27,70,109,127	1,2,3	21.38	6.94	2.68
IVS–FS	Grass	1,2,6,13,21	1:3,5,6, 9,15, 37, 40, 67	1,2,60	22.51	9.75	4.72
	Water	1	1,4	1:3,5			
	Street	1,2,8,12,13,15,16,20,21, 27,31,42,47,49,70,77,97	1,10,15,16,18,19,22, 43,47,49,59,66,70,85,105	1,2,8			
	Roofs	1,2,3,8	1:4,8,14:17,28,35,85,171	1:3,8,11			
	Trees	1,2	1,2	1,2,6			
	Path	1	1	1,14,17			
	Shadow	1	1	1,14,17			

TABLE III
PCS OBTAINED BY PROPOSED FEATURE SELECTION ALGORITHMS WITH VARIOUS CLASSIFIERS FOR SALINAS-A HS DATASET

Method	Class	Selected PCs			Execution time (s)		
		SVM	NB	KNN	SVM	NB	KNN
IDFS	All classes	1:3,5,14,15,37, 63	1:5,9,11,14,15,19:2 2,38,41,52, 91,145,148	1:3,5	10.31	3.52	1.25
IVS–FS	Brocoli_green_weeds_1	1,5	1	1,5	12.59	7.23	3.76
	Corn_senesced_green_weeds	1:3,5,23,24,79, 90	1:5,9,11,14,15, 20,21,32,102,111	1:3,5,8,13,23			
	Lettuce_romaine_4wk	1,2,5,15,16,19, 21,36,66,71,81, 94,96	1:3,7,19,145	1:3,8,15,18:2 0,27,30, 139,166			
	Lettuce_romaine_5wk	1:3,6,7	1	1,3,91			
	Lettuce_romaine_6wk	1:5,13,20,30,63 ,65,106	1:3,6	1,3,5,6,13,14 ,79			
	Lettuce_romaine_7wk	1:5,13,20,30,63 ,65,106	1:3,6	1,3,5,6,13,14 ,79			

datasets. The results of the proposed IDFS and IVS–FS methods have been shown in Tables II–IV for WDC-M, Salinas-A, and Botswana HS datasets, respectively.

For the WDC-M dataset as shown in Table II, the total number of PCs obtained IDFS method using SVM, NB, and KNN as wrappers are 9, 9, and 3, respectively. In contrast, the IVS–FS method is able to obtain a set of PCs for each class of WDC-M dataset. The total number of PCs obtained with the IVS–FS method using SVM, NB, and KNN as wrappers, respectively, can be for each class, such as grass (5, 10, 3), water (1, 2, 4), street (17, 15, 3), roofs (4, 13, 5), trees (2, 2, 3), path (1, 1, 3), and shadow (1, 1, 3). For IVS–FS using SVM, classes,

TABLE IV
PCs OBTAINED BY PROPOSED FEATURE SELECTION ALGORITHMS WITH VARIOUS CLASSIFIERS FOR BOTSWANA HS DATASET

Method	Class	Selected PCs			Execution time (s)		
		SVM	NB	KNN	SVM	NB	KNN
IDFS	All classes	1:6,13,27	1:6,9,58,71	1:4	32.47	5.61	2.15
IVS–FS	Water	1,2,11	1,2	1,2	136.25	15.50	10.32
	Hippo grass	1:4,9,19,22,23,29,30,70	1:5,9,20,24,26,49, 79	1:4,6,8			
	Floodplain grasses1	1:5,12,14,22,26	1:9,14,15,26,40	1:3,5			
	Floodplain grasses2	1:4,11,13,24	1:6,9:13,58,126	1:5,9			
	Reeds1	1:8,18,20	1:6,9,17,46,48,58, 92	1:3			
	Riparian	1:4,6,9,11,12,33,35,38,39,104, 110,118	1:7,9,15,19,35,128, 136	1:4,6			
	Firescar2	1:4,7,8,19,75,87	1,2,6,24	1:3,5			
	Island interior	1:4,6,15,21,41,43,44,79	1:4,9,18,20,24,31,45, 93:95,106,111	1:4,9,91			
	Acacia woodlands	1:6,11,19,23	1:6,12,24,27,32,48, 56,65,85,90,91	1:4,6			
	Acacia shrublands	1:6,9,10,12,25,63,92,98,119,1 20	1:6,8,9,14,15,23, 25:29,32,33,36,39, 41,56,62,64	1:5			
	Acacia grasslands	1:5,7,14,16,18,26,48,61,78,10 0	1:3,5,14,35,55,57,85, 91,93,108	1:5,7,9,11			
	Short mopane	1:3,6:8,38,73,80,82,89,109,12 2,127	1,2,5,14,21,27,28, 35, 43	1,2,4			
	Mixed mopane	1,7,8,11,15,23,24,40,63,98	1,33,46,71,93	1,7			
	Exposed soils	1,7,8,11,15,23,24,40,63,98	1,33,46,71,93	1,7			

namely water, path, and shadow, require only 01 PC, whereas the maximum number of PCs (17 PCs) is required for the street class. For IVS–FS using NB, path and shadow classes are associated with the minimum number of PCs (01 PC), and the street class is associated with the maximum number of PCs (15 PCs). Similarly, for IVS–FS using KNN, the classes namely grass, street, trees, path, and shadow require the minimum number of PCs (03 PCs), whereas the maximum number of PCs (05 PCs) is associated with the roofs class.

From Table III, for the Salinas-A dataset, the total number of PCs obtained by the IDFS method using SVM, NB, and KNN as wrappers are 8, 19, and 4, respectively. In contrast, the IVS–FS method is able to obtain a set of PCs for each class of the Salinas-A dataset. The total number of PCs obtained with the IVS–FS method using SVM, NB, and KNN as wrappers, respectively, can be for each class namely Brocoli_green _weeds_1 (2, 1, 2), Corn_senesced_green_weeds (8, 14, 7), Lettuce_romaine_4wk (13, 6, 12), Lettuce_romaine _5wk (5, 1, 3), Lettue_romaine_6wk (11, 4, 7), and Lettuce_ romaine_7wk (11, 4, 7). For IVS–FS using SVM, the Brocoli_green_weeds_1 class requires only 02 PCs, whereas the maximum number of PCs (13 PCs) is required for the Lettuce_romaine_4wk class. For IVS–FS using NB, Brocoli_green_weeds_1 and Lettuce_romaine_5wk classes require only 01 PC, and the Corn_senesced_green_weeds class is associated with the maximum number of PCs (14 PCs). Similarly, for IVS–FS using KNN, the Brocoli_green_weeds_1 class requires only 02 PCs, whereas the maximum number of PCs (12 PCs) is associated with the Lettuce_romaine_4wk class.

From Table IV, for the Botswana dataset, the total number of PCs obtained by the IDFS method using SVM, NB, and KNN as wrappers are 8, 9, and 4, respectively. In contrast, the IVS–FS method is able to obtain a set of PCs for each class of the Botswana dataset. The total number of PCs obtained with the IVS–FS method using SVM, NB, and KNN as wrappers, respectively, can be for each class namely water (3, 2, 2), hippo grass (11, 11, 6), floodplain grasses1 (9, 13, 4), floodplain grasses2 (7, 13, 6), reeds1 (10, 12, 3), riparian (15, 13, 5), firescar2 (9, 4, 4), island interior (11, 15, 6), Acacia woodlands (9, 16, 5), Acacia shrublands (15, 24, 5), Acacia grasslands (14, 12, 8), short mopane (14, 9, 3), mixed mopane (10, 5, 2), and exposed soils (10, 5, 2). For IVS–FS using SVM, the water class requires only 03 PCs, whereas the maximum number of PCs (15 PCs) is required for the riparian and Acacia shrublands classes. For IVS–FS using NB, the water class requires only 02 PCs, and the Acacia shrublands class is associated with the maximum number of PCs (24 PCs). Similarly, for IVS–FS using KNN, water, mixed mopane, and exposed soils classes require only 02 PCs, whereas the maximum number of PCs (08 PCs) is associated with the Acacia grasslands class.

In all three HS datasets, the increase in the number of PCs for the identification of a class is dependent on the complexity of the class for the used wrapper classifier. The IVS–FS method is superior to the IDFS method. The important point noteworthy here is that classwise PCs obtained by the IVS–FS method are SOTA to improve the classification results of the HS datasets. The selection of PCs for each class of the given HS dataset will be a one-time exercise. Hence, the execution time of the IVS–FS method is relatively more, which may be acceptable in the context of offline experiments.

B. Results of Proposed SSC Approach

This section presents the classification results of the proposed SSC approach obtained by using additional ML algorithms, such as SVM and KNN, in addition to the NB classifier as a wrapper

TABLE V
CLASSIFICATION ACCURACIES IN PERCENTAGE FOR DIFFERENT CLASSIFIERS FOR WDC-M HS DATASET

Approach	Various classification methods and SOTA				Conventional			IVS		
Method	SVM (1:3PCs)	NB (1:3PCs)	KNN (1:3PCs)	3-DCNN	SVM–AFFT–SSC	NB–AFFT–SSC	KNN–AFFT–SSC	IVS–SVM–AFFT–SSC	IVS–NB–AFFT–SSC	IVS–KNN–AFFT–SSC
OA (%)	99.45±0.01	99.48±0.02	99.44±0.01	99.02±0.26	99.72±0.01	99.56±0.03	99.44±0.01	**99.84±0.01**	99.61±0.12	99.59±0.01
AA (%)	93.02±0.09	92.16±0.49	92.89±0.14	92.66±1.13	96.51±0.17	92.44±0.49	92.89±0.14	**97.79±0.02**	94.62±0.42	94.85±0.28
K× (%)	99.23±0.01	99.27±0.02	99.22±0.01	98.61±0.36	99.60±0.02	99.37±0.04	99.22±0.01	**99.77±0.02**	99.45±0.17	99.43±0.01
Grass	99.88±0.01	99.91±0.01	99.77±0.02	99.91±0.01	99.86±0.02	99.93±0.02	99.77±0.02	99.93±0.01	99.95±0.02	99.88±0.01
Water	100±0.00	100±0.00	100±0.00	100±0.00	100±0.00	100±0.00	100±0.00	100±0.00	100±0.00	100±0.00
Street	100±0.00	99.59±0.01	100±0.00	96.92±1.39	100±0.00	99.90±0.05	100±0.00	100±0.00	99.54±0.40	100±0.00
Roofs	64.56±0.63	97.47±0.63	72.78±0.01	78.27±6.96	88.61±1.26	98.73±0.64	72.78±0.01	97.47±1.90	96.20±3.17	79.11±0.01
Trees	99.82±0.01	99.63±0.01	99.88±0.01	99.39±0.18	99.88±0.06	99.70±0.01	99.88±0.01	99.88±0.01	99.64±0.27	99.76±0.06
Path	99.02±0.01	99.02±0.01	99.02±0.01	95.31±2.78	99.35±0.01	99.34±0.01	99.02±0.01	99.35±0.33	99.35±0.33	99.35±0.01
Shadow	87.88±0.01	49.49±4.04	78.79±0.01	78.79±10.60	87.88±0.01	49.49±4.04	78.79±0.01	87.88±0.01	67.68±5.05	85.86±2.02
Time (s)	0.2	0.01	0.01	32.51	0.15	0.03	0.03	0.29	0.05	0.06

The bold values are the highest values achieved by the method.

to prove the generality of the approach. The implementation of the proposed SSC approach in the conventional classification approach has resulted in methods, such as SVM–AFFT–SSC, NB–AFFT–SSC, and KNN–AFFT–SSC. These methods are fed with the PCs obtained by the IDFS method. Similarly, the proposed SSC approach implemented in the proposed IVS approach has resulted in methods, such as IVS–SVM–AFFT–SSC, IVS–NB–AFFT–SSC, and IVS–KNN–AFFT–SSC. These methods are fed with classwise PCs obtained using the IVS–FS method. The reason for selection of the first three PCs for the classifiers (SVM, NB, and KNN) is that we considered cumulative variance of 99% realized through the first three PCs [39]. A comparison of various classification methods with the first three PCs along with the SOTA classifier 3-DCNN [21], [22], [23] and the SSC methods using the proposed SSC approach for three HS datasets is presented to substantiate the effectiveness of the proposed SSC approach. It may be noted that a detailed study has been carried out to address the failure of 3-DCNN with low percentage of training data (2.5%). With 30% of training data, classification accuracy of 3-DCNN is comparable to the results obtained through the proposed SSC methods using only 2.5% of training data.

The classification results of these classifiers in terms of OA, average accuracy (AA), Kappa coefficient (K), and individual class accuracy are presented in Tables V–VII for the WDC-M, Salinas-A, and Botswana HS datasets, respectively.

From Table V, for the WDC-M dataset, the OA, AA, and Kappa of the SVM–AFFT–SSC method are slightly higher by about 0.27%, 3.49%, and 0.37%, respectively, whereas those of the IVS–SVM–AFFT–SSC method are higher by about 0.39%, 4.77%, and 0.54%, respectively, when compared to those of the conventional SVM classifier with the first three PCs. The OA, AA, and Kappa of the NB–AFFT–SSC method are slightly higher by about 0.08%, 0.28%, and 0.10%, respectively, whereas those of the IVS–NB–AFFT–SSC method are higher by about 0.13%, 2.46%, and 0.18%, respectively, when compared to those of the conventional NB classifier with the first three PCs. In a similar comparison, it is found that the OA, AA, and Kappa of the KNN–AFFT–SSC method and those of KNN with the first three PCs are the same, indicating that there is no improvement, However, the OA, AA, and Kappa of the IVS–KNN–AFFT–SSC method are higher by 0.15%, 1.96%, and 0.21%, respectively, when compared with those of the KNN classifier with the first three PCs.

Similarly, the OA, AA, and Kappa of SVM–AFFT–SSC are 0.7%, 3.85%, and 0.99%, respectively, higher than those of 3-DCNN, while the OA, AA, and Kappa of IVS–SVM–AFFT–SSC are 0.82%, 5.13%, and 1.16%, respectively, higher than those of 3-DCNN. Similarly, the OA and Kappa of NB–AFFT–SSC are higher by 0.54% and 0.76%, whereas AA of NB–AFFT–SSC is lower by 0.22% when compared to those of 3-DCNN. The OA, AA, and Kappa of IVS–NB–AFFT–SSC are higher by 0.59%, 1.96%, and 0.84%, respectively, than those of 3-DCNN. Similarly, the OA, AA, and Kappa of KNN–AFFT–SSC are 0.42%, 0.23%, and 0.61%, respectively, higher than those of 3-DCNN, while the OA, AA, and Kappa of IVS–KNN–AFFT–SSC are 0.57%, 2.19%, and 0.82%, respectively, higher than those of 3-DCNN. The highest improvement in OA (0.82%↑), AA (5.13%↑), and Kappa (1.16%↑) is achieved by the IVS–SVM–AFFT–SSC method when compared with 3-DCNN. In addition, the classification accuracy of the roofs class is significantly improved by about 32.91% with the IVS–SVM–AFFT–SSC method when compared with the SVM classifier with the first three PCs. The classification accuracy of the shadow class is significantly improved by about 18.19% with the IVS–NB–AFFT–SSC method when compared with the NB classifier with the first three PCs. Similarly, there is an improvement in the classification accuracy of the roofs class by about 6.33% with the IVS–KNN–AFFT–SSC method when compared with the KNN classifier with the first three PCs.

From Table VI, for the Salinas-A dataset, the OA, AA, and Kappa of the SVM–AFFT–SSC method are higher by about 0.84%, 0.97%, and 1.06%, respectively, whereas those of the IVS–SVM–AFFT–SSC method are higher by about 1.36%,

TABLE VI
CLASSIFICATION ACCURACIES IN PERCENTAGE FOR DIFFERENT CLASSIFIERS FOR SALINAS-A HS DATASET

Approach	Various classification methods with SOTA				Conventional			IVS		
Method	SVM (1:3PCs)	NB (1:3PCs)	KNN (1:3PCs)	3-DCNN	SVM–AFFT–SSC	NB–AFFT–SSC	KNN–AFFT–SSC	IVS–SVM–AFFT–SSC	IVS–NB–AFFT–SSC	IVS–KNN–AFFT–SSC
OA (%)	98.21±0.01	92.67±0.02	98.11±0.01	98.95±0.20	99.05±0.07	98.92±0.09	98.35±0.04	**99.57**±0.06	98.99±0.04	99.03±0.11
AA (%)	98.13±0.01	93.81±0.06	98.04±0.01	98.80±0.17	99.10±0.01	98.58±0.11	98.24±0.02	**99.61**±0.12	98.67±0.04	98.93±0.07
K× (%)	97.75±0.01	90.87±0.02	97.64±0.01	98.69±0.26	98.81±0.10	98.64±0.12	97.94±0.05	**99.46**±0.07	98.73±0.05	98.78±0.14
Brocoli_green_weeds_1	99.74±0.01	99.49±0.01	99.74±0.01	99.23±0.25	99.74±0.01	99.49±0.25	100±0.00	100±0.00	99.74±0.01	100±0.00
Corn_senesced_green_weeds	97.24±0.01	79.67±0.08	96.72±0.01	98.51±0.37	98.14±0.52	99.85±0.13	97.47±0.15	98.96±0.07	99.93±0.01	98.73±0.19
Lettuce_romaine_4wk	95.94±0.01	92.53±0.32	94.48±0.02	97.73±1.95	98.38±0.01	95.13±0.01	94.48±0.01	98.86±0.81	95.13±0.16	96.10±0.95
Lettuce_romaine_5wk	100±0.00	99.48±0.13	99.93±0.01	99.90±0.1	99.74±0.13	99.93±0.01	100±0.00	99.93±0.07	100±0.00	99.80±0.07
Lettuce_romaine_6wk	100±0.00	97.48±0.30	99.85±0.01	97.77±2.07	100±0.00	99.85±0.01	100±0.00	100±0.00	99.85±0.01	99.55±0.01
Lettuce_romaine_7wk	95.87±0.01	94.24±0.01	97.50±0.01	99.69±0.18	98.62±0.63	97.25±0.25	97.50±0.01	98.87±1.13	97.37±0.01	99.37±0.38
Time (s)	0.25	0.04	0.97	11.71	0.07	0.06	0.01	0.17	0.09	0.05

The bold values are the highest values achieved by the method.

TABLE VII
CLASSIFICATION ACCURACIES IN PERCENTAGE FOR DIFFERENT CLASSIFIERS FOR THE BOTSWANA HS DATASET

Approach	Various classification methods and SOTA				Conventional			IVS		
Method	SVM (1:3PCs)	NB (1:3PCs)	KNN (1:3PCs)	3-DCNN	SVM–AFFT–SSC	NB–AFFT–SSC	KNN–AFFT–SSC	IVS–SVM–AFFT–SSC	IVS–NB–AFFT–SSC	IVS–KNN–AFFT–SSC
OA (%)	78.60±0.12	80.79±0.21	77.28±0.01	85.68±1.04	85.41±0.07	86.92±0.95	82.91±0.06	92.03±0.01	**93.04**±0.18	84.42±0.28
AA (%)	75.65±0.05	81.51±0.20	74.95±0.02	86.04±1.31	82.45±0.11	86.81±0.66	80.59±0.14	91.82±0.05	**93.50**±0.26	82.37±0.17
K× (%)	76.80±0.13	79.18±0.23	75.38±0.01	84.49±1.12	84.17±0.07	85.52±1.33	81.47±0.07	91.36±0.01	**92.46**±0.20	83.12±0.29
Water	99.26±0.72	98.89±0.01	100±0.00	100±0.00	95.56±0.75	98.15±1.85	100±0.00	100±0.00	100±0.00	100±0.00
Hippo grass	71.29±1.98	84.16±0.01	82.18±0.99	87.13±7.15	79.21±0.99	99.01±0.90	89.11±0.01	98.02±0.99	100±0.00	92.08±1.98
Floodplain grasses1	87.65±0.06	93.23±0.40	93.63±0.04	86.06±1.78	96.41±0.01	97.21±0.40	97.21±0.01	97.61±0.79	99.60±0.03	92.03±1.20
Floodplain grasses2	92.56±0.93	80.47±1.86	95.35±0.46	93.49±1.28	96.74±0.46	90.70±0.47	96.28±0.46	95.35±0.93	91.63±2.79	99.07±0.01
Reeds1	83.27±0.37	86.24±0.01	81.04±0.37	86.25±2.84	91.45±0.37	88.10±2.23	90.33±1.85	93.68±1.11	94.80±0.38	83.27±0.74
Riparian	59.11±0.75	51.67±0.02	50.93±0.37	40.89±7.50	72.49±0.37	71.74±3.71	59.48±0.01	73.23±1.12	76.58±7.40	56.14±8.17
Firescar2	79.54±2.70	95.75±0.02	92.66±0.04	93.44±1.20	67.95±1.16	80.70±11.96	84.94±0.02	97.68±1.15	93.44±3.09	91.12±1.16
Island interior	75.86±0.02	78.82±0.01	73.89±2.96	100±0.00	88.67±0.99	84.24±1.47	84.24±0.02	96.06±0.49	91.13±0.50	95.57±3.34
Acacia woodlands	67.20±0.63	71.34±0.63	66.56±0.05	97.13±1.34	89.17±0.01	90.45±1.27	75.80±0.31	90.13±0.63	91.72±0.64	89.81±0.96
Acacia shrublands	76.61±0.40	60.08±0.01	62.10±0.03	96.77±6.55	88.31±0.03	79.03±3.63	77.82±1.21	89.92±0.40	91.13±0.50	77.82±1.21
Acacia grasslands	89.51±0.01	93.44±0.02	92.79±0.03	91.48±3.13	85.57±0.03	95.74±0.99	85.57±0.03	92.13±0.01	94.75±0.99	79.67±3.94
Short mopane	89.50±0.03	80.66±0.01	91.71±0.02	88.40±4.39	91.71±0.60	72.38±1.10	95.03±0.02	83.98±0.01	93.37±1.10	90.06±2.20
Mixed mopane	76.12±0.37	71.64±0.01	55.97±2.24	58.21±0.72	91.04±0.04	84.70±0.37	78.73±0.01	95.52±0.74	94.03±0.01	85.45±0.37
Exposed soils	11.58±0.01	94.74±0.03	10.53±0.01	85.26±11.45	20.00±0.01	83.16±6.31	13.68±2.10	82.11±0.01	96.84±1.05	21.05±1.10
Time (s)	6.18	0.06	0.01	111.80	0.037	0.08	0.01	1.80	0.10	0.10

The bold values are the highest values achieved by the method.

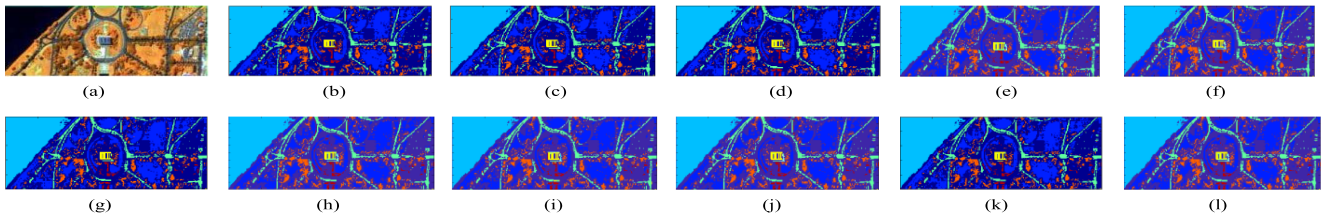

Fig. 3. (a) Portion of WDC-M HS image (RGB). (b) Ground truth, classified images by (c) SVM first three PCs, (d) NB first three PCs, (e) KNN first three PCs, (f) SVM–AFFT–SSC, (g) NB–AFFT–SSC, (h) KNN–AFFT–SSC, (i) 3-DCNN, (j) IVS–SVM–AFFT–SSC, (k) IVS–NB–AFFT–SSC, and (l) IVS–KNN–AFFT–SSC.

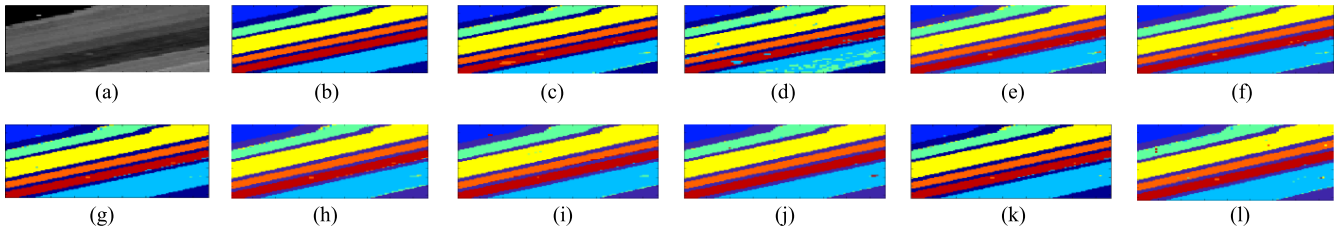

Fig. 4. (a) Salinas-A HS image (gray scale). (b) Ground truth, classified images by (c) SVM first three PCs, (d) NB first three PCs, (e) KNN first three PCs, (f) SVM–AFFT–SSC, (g) NB–AFFT–SSC, (h) KNN–AFFT–SSC, (i) 3-DCNN, (j) IVS–SVM–AFFT–SSC, (k) IVS–NB–AFFT–SSC, and (l) IVS–KNN–AFFT–SSC.

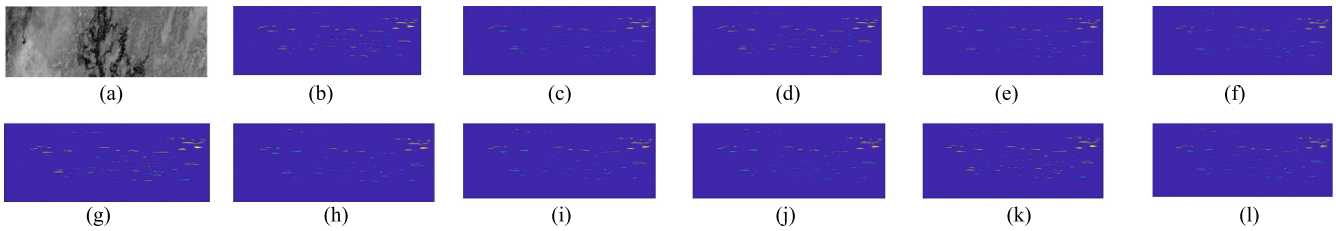

Fig. 5. (a) Botswana HS image (gray scale). (b) Ground truth, classified images by (c) SVM first three PCs, (d) NB first three PCs, (e) KNN first three PCs, (f) SVM–AFFT–SSC, (g) NB–AFFT–SSC, (h) KNN–AFFT–SSC, (i) 3-DCNN, (j) IVS–SVM–AFFT–SSC, (k) IVS–NB–AFFT–SSC, and (l) IVS–KNN–AFFT–SSC.

1.48%, and 1.71%, respectively, when compared to those of the conventional SVM classifier with the first three PCs. The OA, AA, and Kappa of the NB–AFFT–SSC method are significantly higher by about 6.25%, 4.77%, and 7.77%, respectively, whereas those of the IVS–NB–AFFT–SSC method are significantly higher by about 6.32%, 4.86%, and 7.86%, respectively, when compared to those of the conventional NB classifier with the first three PCs. In a similar comparison, it is observed that the OA, AA, and Kappa of the KNN–AFFT–SSC method are higher by about 0.24%, 0.2%, and 0.3% respectively, whereas those of the IVS–KNN–AFFT–SSC are higher by 0.92%, 0.89%, and 1.14%, respectively, when compared to those of the conventional KNN classifier with the first three PCs.

Further, the OA, AA, and Kappa of SVM–AFFT–SSC are 0.10%, 0.30%, and 0.12%, respectively, higher than those of 3-DCNN, while the OA, AA, and Kappa of IVS–SVM–AFFT–SSC are 0.62%, 0.81%, and 0.77%, respectively, higher than those of 3-DCNN. However, the NB–AFFT–SSC and KNN–AFFT–SSC methods are inferior to 3-DCNN in terms of classification performance. The OA and Kappa of IVS–NB–AFFT–SSC are higher by 0.04% and 0.04%, whereas AA of IVS–NB–AFFT–SSC is lower by 0.13% when compared to those of 3-DCNN. The OA, AA, and Kappa of IVS–KNN–AFFT–SSC are higher by 0.08%, 0.13%, and 0.09%, respectively, than those of 3-DCNN. The highest improvement in OA (0.62%↑), AA (0.81%↑), and Kappa (0.77%↑) is achieved by the IVS–SVM–AFFT–SSC method when compared with 3-DCNN. In addition, the classification accuracy of the Lettuce_romaine_7wk class is improved by about 3% with the IVS–SVM–AFFT–SSC method when compared with the SVM classifier with the first three PCs. The classification accuracy of the Corn_senesced_green_weeds class is significantly improved by about 20.26% with the IVS–NB–AFFT–SSC method when compared with the NB classifier with the first three PCs. Similarly, there is an improvement in the classification accuracy of the Lettuce_romaine_4wk class by about 1.62% with the IVS–KNN–AFFT–SSC method when compared with the KNN classifier with the first three PCs.

From Table VII, for the Botswana dataset, the OA, AA, and Kappa of the SVM–AFFT–SSC method are significantly higher by about 6.81%, 6.80%, and 7.37%, respectively, whereas those of the IVS–SVM–AFFT–SSC method are tremendously higher by about 13.43%, 16.17%, and 14.56%, respectively, when

compared to those of the conventional SVM classifier with the first three PCs. The OA, AA, and Kappa of the NB–AFFT–SSC method are higher by about 6.13%, 5.30%, and 6.34%, respectively, whereas those of the IVS–NB–AFFT–SSC method are significantly higher by about 12.25%, 11.99%, and 13.28%, respectively, when compared to those of the conventional NB classifier with the first three PCs. In a similar comparison, it is seen that the OA, AA, and Kappa of the KNN–AFFT–SSC method are higher by about 5.63%, 5.64%, and 6.09%, respectively, than those of the KNN classifier with the first three PCs. Also, the OA, AA, and Kappa of the IVS–KNN–AFFT–SSC method are higher by 7.14%, 7.42%, and 7.74%, respectively, when compared with those of the KNN classifier with the first three PCs.

Similarly, the OA, AA, and Kappa of SVM–AFFT–SSC are 0.27%, 3.59%, and 0.32%, respectively, lower than those of 3-DCNN, while the OA, AA, and Kappa of IVS–SVM–AFFT-SSC are significantly higher by 6.35%, 5.78%, and 6.87%, respectively, than those of 3-DCNN. Similarly, the OA, AA, and Kappa of NB–AFFT–SSC are, respectively, higher by 1.24%, 0.77%, and 1.03%, when compared to those of 3-DCNN. The OA, AA, and Kappa of IVS–NB–AFFT–SSC are significantly higher by 7.36%, 7.46%, and 7.97%, respectively, than those of 3-DCNN. However, the performance of both KNN–AFFT–SSC and IVS–KNN–AFFT–SSC methods is inferior to 3-DCNN. The highest improvement in OA (7.36%↑), AA (7.46%↑), and Kappa (7.97%↑) is achieved by the IVS–NB–AFFT—SSC method when compared with 3-DCNN. In addition, the classification accuracy of the exposed soils class is tremendously improved by about 70.53% with the IVS–SVM–AFFT–SSC method when compared with the SVM classifier with the first three PCs. The classification accuracy of the riparian class is significantly improved by about 24.91% with the IVS–NB–AFFT–SSC method when compared with the NB classifier with the first three PCs. Similarly, there is an improvement observed in the classification accuracy of the exposed soils class by about 10.52% with the IVS–KNN–AFFT–SSC method when compared with the KNN classifier with the first three PCs.

The execution times of the IVS-based SSC methods (IVS–SVM–AFFT–SSC, IVS–NB–AFFT–SSC, and IVS–KNN–AFFT–SSC), as can be seen from Tables V to VII, for the classification of three HS datasets, are slightly higher when compared to their conventional counterparts and also the classifiers with the first three PCs and it is dependent on the number of classes present in the HS dataset. The RGB/gray scale image, the ground truth, and the classified images are obtained by various classification methods including 3-DCNN and the methods based on the proposed SSC approach for the WDC-M dataset, the Salinas-A dataset, and the Botswana dataset are shown in Figs. 3, 4, and 5, respectively.

VI. Conclusion

The proposed SSC approach based on the NB classifier and the AFFT yielded superior classification results for three real HS datasets. The generality of the approach with the well-known additional ML classifiers, such as SVM and KNN, has been demonstrated. It is found that the NB classifier as a wrapper in the proposed SSC approach continues to exhibit relatively better performance compared to the SVM and the KNN classifiers for the Botswana dataset. On the contrary, the SVM classifier as a wrapper in the SSC approach exhibits relatively better performance than the NB and the KNN classifiers for WDC-M and Salinas-A datasets. In the overall sense, the IVS–SVM–AFFT–SSC method yielded the highest accuracy, achieving impressive OA, AA, and Kappa (with percentage of increase) of 99.84% (0.82%↑), 97.79% (5.13%↑), and 99.77% (1.16%↑) for the WDC-M dataset, 99.57% (0.62%↑), 99.61% (0.81%↑), and 99.46% (0.77%↑) for the Salinas-A dataset, whereas the IVS–NB–AFFT–SSC method achieved OA, AA, and Kappa of 93.04% (7.36%↑), 93.50% (7.46%↑), and 92.46% (7.97%↑) for the Botswana image (when compared to the SOTA 3-DCNN method). The novel approach of using the IVS–FS method to obtain classwise PCs contributed significantly to the superior accuracy achieved by the IVS–NB–AFFT–SSC and IVS–SVM–AFFT–SSC methods. Notably, this approach not only enhanced classification accuracy but also provided users with the ability to concentrate on a specific set of PCs for the class of their interest, further improving the applicability and usefulness of the approach.

Acknowledgment

The authors would like to thank D. A. Landgrebe from the Purdue University for providing the HS data. The authors are grateful to Sankaran M, the Director of U. R. Rao Satellite Centre (URSC), Bengaluru, India, Venkatagovinda Rao D, CGM, Facilities, Govindan P, GM, ETF, and Dinesh Chandra, DGM, ETF-1 for encouraging such research activity in the centre. The authors wish to thank the following individuals for their support: Puneet Sharma and Sudhakar from CATVAC, URSC, and Kantha P from the URSC Library.

References

[1] D. A. Landgrebe, *Signal Theory Methods in Multispectral Remote Sensing*, vol. 24. Hoboken, NJ, USA: Wiley, 2003.

[2] L. Samaniego, A. Bárdossy, and K. Schulz, "Supervised classification of remotely sensed imagery using a modified *k*-NN technique," *IEEE Trans. Geosci. Remote Sens.*, vol. 46, no. 7, pp. 2112–2125, Jun. 2008.

[3] M. Fauvel, "Spectral and spatial methods for the classification of urban remote sensing data," doctoral dissertation, Institut National Polytechnique de Grenoble-INPG, Université d'Islande, Reykjavik, Iceland, 2007.

[4] C. Hernández-Espinosa, M. Fernández-Redondo, and J. Torres-Sospedra, "Some experiments with ensembles of neural networks for classification of hyperspectral images," in *Advances in Neural Networks*. Berlin, Germany: Springer, Aug. 2004, pp. 912–917.

[5] H. Zhou, Z. Mao, and D. Wang, "Classification of coastal areas by airborne hyperspectral image," in *Opt. Technol. Atmos., Ocean, Environ. Stud.*, May 2005, pp. 471–476.

[6] L. Bruzzone and B. Demir, "A review of modern approaches to classification of remote sensing data," in *Land Use and Land Cover Mapping in Europe: Practices & Trends*. Dordrecht, The Netherlands: Springer, Jan. 2014, pp. 127–143.

[7] A. Zare and K. C. Ho, "Endmember variability in hyperspectral analysis: Addressing spectral variability during spectral unmixing," *IEEE Signal Process. Mag.*, vol. 31, no. 1, pp. 95–104, Dec. 2013.

[8] M. Khodadadzadeh, J. Li, A. Plaza, H. Ghassemian, J. M. Bioucas-Dias, and X. Li, "Spectral–spatial classification of hyperspectral data using local and global probabilities for mixed pixel characterization," *IEEE Trans. Geosci. Remote Sens.*, vol. 52, no. 10, pp. 6298–6314, Mar. 2014.
[9] Y. Gu, T. Liu, X. Jia, J. A. Benediktsson, and J. Chanussot, "Nonlinear multiple kernel learning with multiple-structure-element extended morphological profiles for hyperspectral image classification," *IEEE Trans. Geosci. Remote Sens.*, vol. 54, no. 6, pp. 3235–3247, Jan. 2016.
[10] B. Demir and L. Bruzzone, "Histogram-based attribute profiles for classification of very high resolution remote sensing images," *IEEE Trans. Geosci. Remote Sens.*, vol. 54, no. 4, pp. 2096–2107, Dec. 2015.
[11] T. Lu, S. Li, L. Fang, Y. Ma, and J. A. Benediktsson, "Spectral–spatial adaptive sparse representation for hyperspectral image denoising," *IEEE Trans. Geosci. Remote Sens.*, vol. 54, no. 1, pp. 373–385, Aug. 2015.
[12] H. Yuan and Y. Y. Tang, "Sparse representation based on set-to-set distance for hyperspectral image classification," *IEEE J. Sel. Topics Appl. Earth Observ. Remote Sens.*, vol. 8, no. 6, pp. 2464–2472, Jun. 2015.
[13] W. Li, S. Prasad, and J. E. Fowler, "Hyperspectral image classification using Gaussian mixture models and Markov random fields," *IEEE Geosci. Remote Sens. Lett.*, vol. 11, no. 1, pp. 153–157, Apr. 2013.
[14] X. Kang, S. Li, L. Fang, M. Li, and J. A. Benediktsson, "Extended random walker-based classification of hyperspectral images," *IEEE Trans. Geosci. Remote Sens.*, vol. 53, no. 1, pp. 144–153, May 2014.
[15] M. Golipour, H. Ghassemian, and F. Mirzapour, "Integrating hierarchical segmentation maps with MRF prior for classification of hyperspectral images in a Bayesian framework," *IEEE Trans. Geosci. Remote Sens.*, vol. 54, no. 2, pp. 805–816, Aug. 2015.
[16] Z. Miao and W. Shi, "A new methodology for spectral—spatial classification of hyperspectral images," *J. Sensors*, vol. 2016, Nov. 2016, Art. no. 1538973.
[17] F. Zhou, R. Hang, Q. Liu, and X. Yuan, "Hyperspectral image classification using spectral—spatial LSTMs," *Neurocomputing*, vol. 328, pp. 39–47, Feb. 2019.
[18] S. Li, W. Song, L. Fang, Y. Chen, P. Ghamisi, and J. A. Benediktsson, "Deep learning for hyperspectral image classification: An overview," *IEEE Trans. Geosci. Remote Sens.*, vol. 57, no. 9, pp. 6690–6709, Sep. 2019.
[19] L. Zhang and L. Zhang, "Artificial intelligence for remote sensing data analysis: A review of challenges and opportunities," *IEEE Geosci. Remote Sens. Mag.*, vol. 10, no. 2, pp. 270–294, Jun. 2022.
[20] M. E. Paoletti, J. M. Haut, J. Plaza, and A. Plaza, "Deep learning classifiers for hyperspectral imaging: A review," *ISPRS J. Photogramm. Remote Sens.*, vol. 158, pp. 279–317, Dec. 2019.
[21] A. Qin et al., " Distance constraint-based generative adversarial networks for hyperspectral image classification," *IEEE Trans. Geosci. Remote Sens.*, vol. 61, pp. 1–16, May 2023.
[22] Y. Li, H. Zhang, and Q. Shen, "Spectral–spatial classification of hyperspectral imagery with 3D convolutional neural network," *Remote Sens.*, vol. 9, no. 1, pp. 67–87, Jan. 2017.
[23] Z. Li et al., "Spectral-learning based transformer network for the spectral super-resolution of remote sensing degraded images," *IEEE Geosci. Remote Sens. Lett.*, vol. 20, 2023, Art. no. 5505705.
[24] T. Wang, H. Liu, and J. Li, "Spectral–spatial classification of few shot hyperspectral image with deep 3-D convolutional random Fourier features network," *IEEE Trans. Geosci. Remote Sens.*, vol. 60, 2022, Art. no. 5532318.
[25] S. Jia, S. Jiang, Z. Lin, N. Li, M. Xu, and S. Yu, "A survey: Deep learning for hyperspectral image classification with few labeled samples," *Neurocomputing*, vol. 448, pp. 179–204, Aug. 2021.
[26] S. K. Roy, J. M. Haut, M. E. Paoletti, S. R. Dubey, and A. Plaza, "Generative adversarial minority oversampling for spectral–spatial hyperspectral image classification," *IEEE Trans. Geosci. Remote Sens.*, vol. 60, pp. 1–15, 2022.
[27] Y. Cheng, D. Wang, P. Zhou, and T. Zhang, "A survey of model compression and acceleration for deep neural networks," *IEEE Signal Process. Mag., Special Issue Deep Learn. Image Understand.*, pp. 1–10, 2020
[28] S. B. Mangal and V. Goyal, "Text news classification system using Naive Bayes classifier," *Int. J. Eng. Sci.*, vol. 3, pp. 209–213, Dec. 2014.
[29] S. Russell and P. Norvig, *Artificial Intelligence: A Modern Approach*, 4th ed. New Jersey, NJ, USA: Prince Hall, 2020.
[30] Y. Chen, N. M. Nasrabadi, and T. D. Tran, "Hyperspectral image classification using dictionary-based sparse representation," *IEEE Trans. Geosci. Remote Sens.*, vol. 49, no. 10, pp. 3973–3985, May 2011.
[31] L. Fang, S. Li, X. Kang, and J. A. Benediktsson, "Spectral–spatial hyperspectral image classification via multiscale adaptive sparse representation," *IEEE Trans. Geosci. Remote Sens.*, vol. 52, no. 12, pp. 7738–7749, May 2014.
[32] MultiSpec, 1995. Accessed: Jul. 1, 2020. [Online]. Available: https://engineering.purdue.edu/∼biehl/MultiSpec/hyperspectral.html
[33] Grupo De Inteligencia Computacional, 2014. Accessed: Feb. 10, 2020. [Online]. Available: http://www.ehu.eus/ccwintco/index.php/Hyperspectral_Remote_Sensing_Scenes#Salinas-A_scene
[34] Grupo De Inteligencia Computacional, 2014. Accessed: Jun. 6, 2020. [Online]. Available: http://www.ehu.eus/ccwintco/index.php/Hyperspectral_Remote_Sensing_Scenes#Botswana
[35] B.-C. Kuo, H.-H. Ho, C.-H. Li, C.-C. Hung, and J.-S. Taur, "A kernel-based feature selection method for SVM with RBF kernel for hyperspectral image classification," *IEEE J. Sel. Topics Appl. Earth Observ. Remote Sens.*, vol. 7, no. 1, pp. 317–326, Jan. 2014.
[36] M. Pal, T. B. Charan, and A. Priya, "*k*-nearest neighbour-based feature selection using hyperspectral data," *Remote Sens. Lett.*, vol. 12, no. 2, pp. 132–141, 2021.
[37] A. K. Singh, "Band selection algorithms and heterogeneous multi-classifier schemes for enhanced classification accuracy of hyperspectral images," Ph.D. dissertation, Coventry Univ., Coventry, U.K., 2019.
[38] X. Huang, Q. Lu, L. Zhang, and A. Plaza, "New postprocessing methods for remote sensing image classification: A systematic study," *IEEE Trans. Geosci. Remote Sens.*, vol. 52, no. 11, pp. 7140–7159, Mar. 2014.
[39] H. Wang, W. Li, X. Chen, and J. Niu, "Hyperspectral classification based on coupling multiscale super-pixels and spatial spectral features," *IEEE Geosci. Remote Sens. Lett.*, vol. 19, pp. 1–5, 2022.

Arvind Kumar Singh received the B.E. degree in electronics and communication engineering from the Vikram University, Ujjain, India, in 1996, the M.Tech. degree in digital communication engineering from the M.S. Ramaiah Institute of Technology, Bangalore, India, in 2006, and the Ph.D. degree in band selection algorithms and heterogeneous multi-classifier schemes for enhanced classification accuracy of hyperspectral images from Coventry University, Coventry, U.K., in 2020.

He is currently a Scientist-SG and a Manager with the CATVAC, U. R. Rao Satellite Centre, Indian Space Research Organisation, Bengaluru, India. He has been a part of the Thermovac tests on the prestigious Chandrayaan-3 spacecraft. His research interests include digital image processing and remote sensing.

Dr. Singh is the recipient of "ISRO Team Excellence Award" for the "Realization of Liquid Nitrogen Cooled Cryo Target for Extreme Low Temperatures on Meteorological Payload Patches."

Renuvenkataswamy Sunkara (Graduate Student Member, IEEE) received the B.Tech. degree in electronics and communication engineering from the Jawaharlal Nehru Technological University, Kakinada, India, in 2009, and the M.Tech. degree in VLSI design and embedded systems from the Reva University, Bengaluru, India, in 2022.

He is currently a Scientist-SC with the U. R. Rao Satellite Centre, Indian Space Research Organisation, Bengaluru, India. He has been a part of Thermovac tests on the prestigious Chandrayaan-3 spacecraft. His research interests include hyperspectral image processing, artificial intelligence, and machine learning.

Mr. Sunkara was a recipient of two prestigious ISRO Team Excellence awards for the year 2015. He was the recipient of the Best Student Award from the Reva University for his best contribution. He was also the recipient of the Best Paper Award at the ICDCECE—2022 conference.

Govind R. Kadambi received the B.E. degree in electronics and communication engineering from the University of Mysore, Mysore, India, in 1978, and the M.S. and Ph.D. degrees in antenna engineering from the Indian Institute of Technology (IIT), Madras, India, in 1983 and 1993, respectively.

Between 1978 and 1994, he was at the IIT, Kharagpur, IIT, Madras, and Aeronautical Development Agency, Bangalore, India. During 1995–2006, he was associated at various Technology Development Organizations in Canada and USA like S.G. Microwaves (Canada), Centurion Wireless Technologies (USA), Interdigital Communications (USA), and Apple Inc. (USA). He returned to India in 2006. Since then, he has been initially with Ramaiah School of Advanced Studies (RSAS), Bengaluru, India and now with Ramaiah University of Applied Sciences (RUAS), Bengaluru. He held the posts of the HoD, Dean, and Deputy Director of the RSAS. Since the formation of RUAS in 2013, he has been the Pro Vice-Chancellor (Research) of the RUAS. He has guided several students for their Ph.D., and currently many students are pursuing their research degree under his supervision. He has been granted 24 U.S. patents and 17 other international patents from China, Korea, Japan, Germany, and Europe. He has filed 18 Indian patent applications. He has authored/coauthored more than 120 research publications in international journals and conferences.

Dr. Kadambi was the Reviewer of IEEE TRANSACTIONS ON ANTENNAS AND PROPAGATION. He has been the Chairman and Invited Speaker at several International Conferences in the USA. He has been the Principal Investigator and Co-Principal Investigator for a number of sponsored research projects funded by the Government of India. Recently, he was selected as the Fellow of KSTA, GoK for the year 2020–21.

Vasile Palade (Senior Member, IEEE) received the M.Eng. degree from the Technical University of Bucharest, Bucharest, Romania, in 1988, and the Ph.D. degree from the University of Galati, Galati, Romania, in 1999.

He is currently a Professor of Artificial Intelligence and Data Science with the Centre for Computational Sciences and Mathematical Modelling, Coventry University, Coventry, U.K. He previously worked with the Department of Computer Science, University of Oxford, Oxford, U.K., and the University of Galati, Galati, Romania. His research interests include machine learning and applications, including deep learning and neural networks, various nature inspired optimization algorithms, computer vision, and natural language processing.

Prof. Palade is an Associate Editor for several journals, such as IEEE TRANSACTIONS ON NEURAL NETWORKS AND LEARNING SYSTEMS, *Neural Networks*, and *Journal of Big Data*. He has delivered keynote talks at international conferences on machine learning and applications.